Forum Acusticum 2011 - Aalborg - Denmark

On the 1D wave propagation in wind instruments with a smooth profile

Thomas Hélie and Thomas Hézard
IRCAM - CNRS UMR 9912-UMPC, 1 place Igor Stravinsky, 75004 Paris, France.

Rémi Mignot
Institut Langevin, ESPCI ParisTech, 10, rue Vauquelin, 75005 Paris, France.

Denis Matignon
Universite de Toulouse, ISAE 10, av. E. Belin. BP 54032, 31055 Toulouse Cedex 4, France.

Summary
Due to the simple properties of plane waves, non lossy straight pipes and their concatenation have been extensively used to compute acoustic transfer functions from bore profiles of wind instruments (input impedance, transmittance, etc). This is also the case for real-time simulations: introducing travelling waves has led to the well-known digital waveguides formalism. Nevertheless, such discontinuous concatenations involve impulse responses composed of pulse trains of Dirac measures, which are structurally unrealistic for smooth bores. Similarly, continuous but non smooth approximations based on conical segments involve discontinuous pulse trains of damped exponentials. This invited paper presents an overview of results that have been elaborated to weaken such artifacts and increase realism, while preserving most of the worthwhile properties of straight pipes. The key steps are based on the use of: (1) a refined 1D wave equation (curvilinear horn equation) based on an isobar map rectification; (2) smooth (C1-regular) junctions of constant-flared acoustic pipes; (3) a radiation model which is compatible with (1); (4) visco-thermal losses. It allows to recover a standard matrix formalism to compute impedances and transmittances of smooth bore parts that yield accurate results. It still make definitions of travelling waves and digital waveguide-like structures possible for the simulation. Finally, by representing smooth bores by very few flared segments (compared to many straight or conical pipes), such descriptions (with a few parameters) are an interesting alternative to optimize wind instrument bores w.r.t. some criteria (target shape or impedance, harmonicity, etc).

PACS no. 43.75.Fg, 43.75.Ef, 43.20.Mv

1. Introduction

This paper focuses on some possible refinements of 1D acoustic models in order to compute accurate input impedances for wind instrument resonators, and especially, smooth horns. It is organized as follows. In sections 2 to 5, we recall some appropriate models and investigate on the *influence of* (§ 2) the choice of the wave-shape assumption in the horn equation, (§ 3) the geometric regularity at junctions in piecewise segment modelling, (§ 4) the radiation impedance and (§ 5) visco-thermal losses. These studies are illustrated on an academic horn profile. Section 6 presents results on a trombone bell, the profile and the input impedance of which have been measured.

Along all this paper, physical constants are the air mass density $\rho_0 = 1.18\,\mathrm{Kg.m^{-3}}$ and the sound celerity $c_0 = 346.63$, deduced from the calibration of the impedance sensor [1] for the measured trombone bell.

The *academic* flared profile $R^\dagger$ used in sections 2-5 is chosen such that boundaries coordinates (z, R) matches with those of the trombone bell ($z_0 = 0$, $R_0^\star = 10.4 \times 10^{-3}$m, $z^\star = 568 \times 10^{-3}$m, $R^\star = 110 \times 10^{-3}$m), with a null slope at $z = 0$. A simple polynomial model which satisfies these properties is given by

$$R^\dagger : z \in [0, z^\star] \mapsto R_0 + \left(R^\star - R_0\right)\left(\frac{z}{z^\star}\right)^{10}. \qquad (1)$$

2. Horn equation and isobars

2.1. Uni-dimensional models and geometry

The first uni-dimensional model of the lossless acoustic propagation in axisymmetric pipes with profile $z \mapsto R(z)$ is due to [2, 3]. It is usually called *"horn equation"* or *"Webster equation"* [4] and is given by

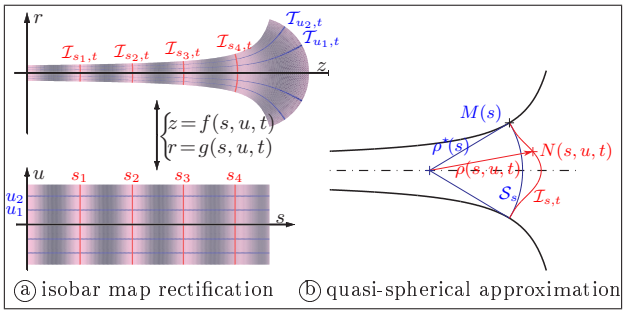

Figure 1. Isobar map rectification and approximation

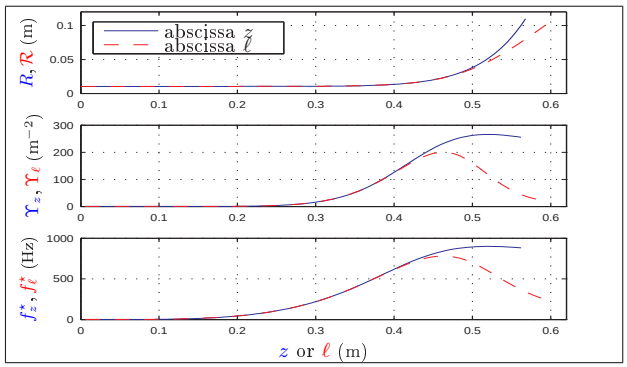

Figure 2. Comparisons on the reference profile.

$$\Big(\partial_z^2+2\frac{R'(z)}{R(z)}\partial_z-\frac{1}{c_0^2}\partial_t^2\Big)p(z,t)=0, \tag{2}$$

$$\Big(\partial_z^2-\Upsilon(z)-\frac{1}{c_0^2}\partial_t^2\Big)\big[R(z)p(z,t)\big]=0,\ \text{with}\ \Upsilon=\frac{R''}{R}, \tag{3}$$

or also a conservative form, using the identity $\frac{1}{A(z)}\,\partial_z\big[A(z)\,\partial_z p(z,t)\big] = \big[\partial_z^2+2\frac{R'(z)}{R(z)}\,\partial_z\big]p(z,t)$ in equation 2 ($A=\pi R^2$ is the bore section area).

This model which assumes planar waves has been extensively investigated [5] and its hypotheses periodically revised: spherical wavefronts orthogonal to the bore are assumed in [6, 7], the quasi-sphericity is experimentally confirmed in the low frequency range for horns in [8], ellipsoidal wavefronts are proposed in [9]. Moreover, it has been proved in [10] that every one-parameter acoustic fields obey a *horn equation* for some adapted space variables.

For many wind instruments, transverse modes [11] only appear as small perturbations on a significant frequency range. So, refining horn equations makes sense and can apply to the derivation of accurate characteristic immittances (input impedance, transmittance, etc) and real-time sound synthesis purposes.

2.2. Quasi-sphericity and curvilinear abscissa

In this paper, we consider the model detailed in [12], based on an *exact isobar wave equation* (step ⓐ) from which an *assumption on isobar shapes* (quasi-sphericity at order 2) is inferred and used (step ⓑ).

Step ⓐ For axi-symmetric problems, writing the wave equation $\big[\partial_r^2-\frac{1}{r}\partial_r+\partial_z^2-\frac{1}{c^2}\partial_t^2\big]p(z,r,t)=0$ in a rectified isobar map, by using a coordinate transformation $z=f(s,u,t)$, $r=g(s,u,t)$ such that $p(f(s,u,t),g(s,u,t),t)=\widetilde{p}(s,t)$ does not depend on u (s indexes isobars $\mathcal{I}_{s,t}$, cf. Figure 1 ⓐ)), yields the isobar wave equation $\big[\alpha\partial_s^2+\beta\partial_s+\gamma\partial_s\partial_t-\frac{1}{c_0^2}\partial_t^2\big]\widetilde{p}(s,t)=0$ where α, β, γ depend on f,g and their derivatives.

The change of coordinates can be chosen such that: (i) u and s are orthogonal; (ii) $f(s,-u,t)=f(s,u,t)$, $g(s,-u,t)=-g(s,u,t)$ (symmetry w.r.t. the axis described by $u=0$); (iii) $u=1$ maps to the (motionless) bore profile described by known (time-invariant) functions $f(s,u=1,t)=\mathcal{W}(s)$, $g(s,u=1,t)=\mathcal{R}(s)$.

Using (iii), computations yield $\alpha(s,1,t)=\sqrt{\big(\mathcal{W}'(s)\big)^2+\big(\mathcal{R}'(s)\big)^2}$, $\gamma(s,1,t)=0$. But $\beta(s,1,t)$ cannot be evaluated from the bore profile $(\mathcal{W},\mathcal{R})$ alone: it requires an additional information on the first variations of the field lines near the bore ($\partial_u f$ and $\partial_u g$ at $(s,u=1,t)$). Thus, β is responsible for the coupling between the propagation of the pressure level of isobars and their geometry.

Step ⓑ An assumption providing this *decoupling information* is looked for, preserving the properties:

> **(P1a)** *Isobars are (i) planes in straight pipes, (ii) spherical in cones, (iii) orthogonal to the wall, (iv) quasi-spherical in horns [8], and (v) are not required to be time-invariant.*

The simplest choice is given by (cf. Figure 1 ⓑ):

> **(H1)** *Near the wall ($u=1$), an isobar deviates from its tangent spherical approximation slower than a parabola, that is, $\partial_u^k\zeta(s,1,t)=0$ for $k=0$ (contact), $k=1$ (tangency) and $k=2$ (assumption) for the relative deviation $\zeta(s,u,t)=\frac{\rho(s,u,t)}{\rho^\star(s)}-1$.*

This yields $\beta(s,1,t)=2\alpha(s,1,t)\frac{\mathcal{R}'(s)}{\mathcal{R}(s)}$. As a result:

> **(R1)** *Under hypothesis (H1),* horn equations *2-3 are recovered with $\big(s,\mathcal{R}(s)\big)$ in place of $\big(z,R(z)\big)$, if $\alpha(s,1,t)=1$, that is, if $s=\ell$ is the* curvilinear abscissa *measuring the profile length:*
>
> $$\ell=L(z)=\int_0^z\sqrt{1+\big[R'(z)\big]^2}\,\mathrm{d}z,\quad \mathcal{R}(\ell)=R\big(L^{-1}(\ell)\big). \tag{4}$$
>
> *Similarly, Euler equation for plane waves is recovered in which z is replaced by ℓ (cf. [12, (53)]):*
>
> $$\rho_0\partial_t v=-\partial_\ell p\quad (v\ \text{is the particle velocity}). \tag{5}$$

2.3. Comparisons between z- and ℓ-models

Changing the space variable in the *horn equation* makes some substantial differences appear. Additionally to (P1a), straightforward properties are:

> **(P1b)** *(i) travel lengths are increased for the* curvilinear horn model *compared to the original one (cf. Figure 2); (ii) $|\mathcal{R}'(\ell)|\le 1$ (since $\mathcal{R}'\big(L(z)\big)=\frac{R'(z)}{\sqrt{1+R'(z)^2}}$); (iii) $R'(\ell)=1$ corresponds to a vertical slope in the z-space; (iv) if a profile $z\mapsto R(z)$ ends with an infinite derivative, the* curvilinear horn equation *operates a natural connection with spherical waves.*

For the ℓ-model, parameter Υ which accounts for curvature becomes $\Upsilon_\ell = \frac{\mathcal{R}''}{\mathcal{R}}$ rather than $\Upsilon_z = \frac{R''}{R}$. It can be mapped to a local-in-space cutoff frequency $f^\star = \frac{c_0}{2\pi}\sqrt{\Upsilon}$ (case $\Upsilon \geq 0$), below which travelling waves become evanescent [8]. Figure 2 exhibits that:

(**P1c**) *The curvilinear ℓ-model makes Υ and $f^\star$ lower than for the axial z-model. It also modifies their variation in space.*

Finally, considering ℓ-models rather than z-models modifies (1) the equivalent pipe length, (2) the values of Υ, (3) the shapes of the pipe and Υ, and so, (4) the immittances peak locations, (5) the cutoff frequency.

3. Constant-flared acoustic pipes

The main interests of 1D propagation models are that: (1) immittances can be computed using the transfer matrix method and (2) if a stable travelling wave decomposition is available, digital waveguides formalism makes real-time sound synthesis possible.

3.1. Transfer matrix method

Consider a bore segment governed by equations 5 and 3 with constant parameter $\Upsilon \geq 0$ on $[a,b[$ ($\Upsilon = 0$ for straight and conical pipes, $\Upsilon > 0$ for flared pipes). Denote $L = b - a$ and $X_\ell(s) = \big[\, P(\ell,s)\,,\, U(\ell,s)\,\big]^T$ where P and U are Laplace transforms of signals $t \mapsto p(\ell,t)$ and $t \mapsto \pi\mathcal{R}(\ell)^2 v(\ell,t)$ (assumed to be zero for $t<0$), respectively. Straightforward computations lead to

$$X_b(s) = \mathbf{T}_{b,a}(s)\, X_a(s), \tag{6}$$

where $\mathbf{T}_{b,a}$ has determinant one and is given by $\mathbf{T}_{b,a}(s) = \mathrm{diag}\Big(\frac{L}{\mathcal{R}(b^-)}, \frac{\pi\mathcal{R}(b^-)}{\rho_0 s}\Big)\, \mathbf{M}_{b,a}(s)\, \mathrm{diag}\Big(\frac{\mathcal{R}(a^+)}{L}, \frac{\rho_0 s}{\pi\mathcal{R}(a^+)}\Big)$, and $[\mathbf{M}_{b,a}(s)]_{p,q} = \big(V_{p,q}(s)\big)^T\, \Phi\big(L\Gamma(s)\big)$ with $\Phi(z) = [\cosh z\,,\, \frac{\sinh z}{z}]^T$, $V_{11} = [1\,,\, \sigma(a^+)]^T$, $V_{12} = [0\,,\, -1]^T$, $V_{21}(s) = [\sigma(b^-) - \sigma(a^+)\,,\, \sigma(a^+)\sigma(b^-) - \big(L\Gamma(s)\big)^2]^T$, $V_{22} = [1\,,\, -\sigma(b^-)]^T$, with $\ell \in [a,b[\mapsto \sigma(\ell) = \frac{\mathcal{R}'(\ell)}{\mathcal{R}(\ell)/(L)}$ and where Γ is an analytic continuation over $\mathbb{C}_0^+ = \{s \in \mathbb{C} \,|\, \Re\mathrm{e}(s) > 0\}$ of the positive square-root of

$$\Gamma(s)^2 = \Big(\frac{s}{c}\Big)^2 + \Upsilon. \tag{7}$$

Connecting a sequence of Υ-constant segments ($\Upsilon(\ell) = \Upsilon_n$ on $\ell \in [\ell_{n-1}, \ell_n[$ for $1 \leq n \leq N$) is achieved by preserving the pressure and the air flow continuity at junctions, so that $X_{\ell_N}(s) = \mathbf{T}_{\ell_N,\ell_0}(s)\, X_{\ell_0}(s)$ with

$$\mathbf{T}_{\ell_N,\ell_0} = \mathbf{T}_{\ell_N,\ell_{N-1}}\, \mathbf{T}_{\ell_{N-1},\ell_{N-2}}\, \ldots\, \mathbf{T}_{\ell_1,\ell_0}. \tag{8}$$

(**P2a**) *Because of ℓ and (P1a), equations 6-8 exactly regenerates the standard results for both straight segments ($\ell \equiv z$, $\mathcal{R}(\ell_{n-1}^+) = \mathcal{R}(\ell_n^-)$, $\sigma_\ell = L\mathcal{R}'(\ell)/\mathcal{R}(\ell) = 0$) and conical segments ($\ell \equiv r$, $\sigma(\ell_{n-1}^+) = \sigma(\ell_n^-)$).*

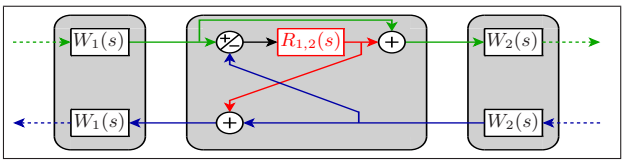

Figure 3. Kelly-Lochbaum structure for segments 1 and 2.

3.2. Kelly-Lochbaum structure

Piecewise cylindrical ⓐ, conical ⓑ and Υ-constant ⓒ bores can be described by digital waveguides structures composed of pairs of travelling operators (also called *propagators*) $W_n(s) = \exp\big[-\Gamma(s)(\ell_n - \ell_{n-1})\big]$, junction transfer quadripoles $Q^j_{n,n+1}(s)$ and load transfer functions at boundaries [13, 14, 15].

Propagators are delays $D_n(s) = \exp(-\tau_n s)$ with $\tau_n = \frac{\ell_n - \ell_{n-1}}{c_0}$ in cases ⓐ-ⓑ ($\Upsilon_n = 0$), combined with the dispersion function W_n/D_n (of a causal stable operator [16]). They monitor some travelling waves inside the pipe. Junction quadripoles monitor the reflections and transmissions of these travelling waves at junctions $\ell = \ell_n$. A nice property [17, 18, 15, 14] for reducing computation load in sound synthesis is:

(**P2b**) *When the geometrical smoothness regularity allowed by piecewise descriptions ⓐ-ⓒ is maximal, that is, discontinuous for ⓐ, continuous for ⓑ and $\mathcal{C}^1$-regular for ⓒ, each quadripole $Q^j(s)$ can be realized by using only one reflection transfer function $R_{n,n+1}(s)$ and three sums: this gives rise to the so-called Kelly-Lochbaum structure recalled in Figure 3.*

Kelly-Lochbaum structure has been originally established in case ⓐ, leading to the *auto-regressive* (AR) filters which are quite used to model the vocal tract [19]. Nevertheless, such AR models suffer from rough approximations. A quite severe one is that AR models are based on frequency-independent radiation impedances. A second one is that they ignore visco-thermal losses, which can be critical for wind musical instruments. A third one is that local-in-space bore discontinuities involve instantaneous (local-in-time) reflections which make the impulse response (IR) of *immittances* (input impedance, transmittance, etc) composed of Dirac pulses rather than the expected smooth responses.

Improving the first two points (addressed in §4-5) regularizes these impulse responses: they conceal the third one from a mathematical point of view. But, from the acoustic point of view, preserving the bore regularity is of main importance, especially when segments lengths are not short enough.

This is why the space discretization δz is usually chosen as $c_0 F_s$ where F_s is sampling frequency: this synchronization with the wave celerity removes artifacts due to discontinuities since, in impulse responses, no zeros appear between each Dirac pulse.

A more accurate alternative consists in increasing the smoothness of the piecewise approximations. To the end, conical bore segments first, and $\mathcal{C}^1$-regular

constant-flared segments second, have been considered. What order of regularity of impulse responses are these descriptions able to preserve ?

3.3. Regularity analysis

Consider a bore loaded by a frequency-independent impedance radiation or an infinitely long last segment. For cases ⓐ-ⓑ, propagators are delays so that:

(P2c) *The regularity of immittance impulse responses are fixed by that of the reflection functions (see $R_{1,2}$ in Figure 3).*

This is still true for case ⓒ since $W_1(s)/D_1(s)$ does not preserve regularity: as $s \to +\infty$ in $\mathbb{C}_0^+$, $W_1(s)/D_1(s) = \exp\left(-(\Gamma_1(s) - \frac{s}{c})c\tau_1\right) = 1 + \frac{c_0^2 \Upsilon_1 \tau_1}{2}\frac{1}{s} + \mathcal{O}(\frac{1}{s^2})$, which contains a direct unit gain.

Table I recalls reflection function formula and illustrates the caricatural approximation of the reference $\mathcal{R}^\dagger$ on $\ell \in [0.3, 0.5[$ with two segments delimited by $\ell_0 = 0.3$, $\ell_1 = 0.4$, $\ell_2 = 0.5$. For the case ⓐ, $R_{1,2}^{ⓐ}(s) = \frac{A_1 - A_2}{A_1 + A_2} = k_{1,2}$ and $r_{1,2}^{ⓑ}(t) = k_{1,2}\,\delta(t)$ (Dirac pulse). For ⓑ, $R_{1,2}^{ⓑ}(s) = \frac{\alpha_{1,2}}{s - \alpha_{1,2}}$ and $r_{1,2}^{ⓑ}(t) = \alpha_{1,2}\exp(\alpha_{1,2}t)\,1_{t\geq 0}$ where $\alpha_{1,2} = \frac{c_0}{2}\left(\frac{\mathcal{R}'(\ell_1^-) - \mathcal{R}'(\ell_1^+)}{\mathcal{R}(\ell_1)}\right)$ (discontinuous IR). For ⓒ, $R_{1,2}^{ⓒ}(s) = \frac{\Gamma_1(s) - \Gamma_2(s)}{\Gamma_1(s) + \Gamma_2(s)} = \frac{\Upsilon_1 - \Upsilon_2}{(\Gamma_1(s) + \Gamma_2(s))^2} = \frac{\Upsilon_1 - \Upsilon_2}{4(s/c)^2} + \mathcal{O}(\frac{1}{s^4})$ as $s \to +\infty$, so that from the initial value theorem, $r_{1,2}(0^+) = \lim_{x\to+\infty} x R_{1,2}(x) = 0$ and $r'_{1,2}(0^+) = \lim_{x\to+\infty} x^2 R_{1,2}(x) = \frac{\Upsilon_1 - \Upsilon_2}{2}$ ($\mathcal{C}^0$ but not $\mathcal{C}^1$ IR).

In conclusion, considering a target smooth profile:

(R2) *$\mathcal{C}^1$-regular junctions of Υ-constant segments define the first piecewise-approximation which preserves the IR continuity, independently of the segment number. Nearly-continuous IR can be obtained by increasing the segment number so that the mesh is refined and the coefficients $\alpha_{n,n+1} = c_0\big(\mathcal{R}'(\ell_n^-) - \mathcal{R}'(\ell_n^+)\big)/\big(2\mathcal{R}(\ell_n)\big)$ become small enough.*

A conjecture for higher continuity degrees is that a $\mathcal{C}^k$-regular profile corresponds to a $\mathcal{C}^{k-1}$-regular IR.

Note that, in the cases ⓐ-ⓑ, defining N segments from a target profile $\mathcal{R}$ is simplify obtained by evaluating $\mathcal{R}$ at chosen abscissa $\ell_{n=0,\ldots,N}$. On the contrary, deriving a $\mathcal{C}^1$-regular piecewise Υ-constant decomposition is not easy. A tool which is specially dedicated to optimize case ⓒ is used in this paper (see [20]).

4. Radiation impedances for horns

The radiation impedance balances the energy which is confined inside the pipe (a) and the radiated part (b). In the frequency ranges where the behaviour (a) largely dominates, the resonances quality is high (making self-oscillations and note emissions easier).

Tuning the trade-off between resonances quality and the radiated sound power (especially for modern instruments) makes the radiation impedance study crucial. Several models, compatible with straight

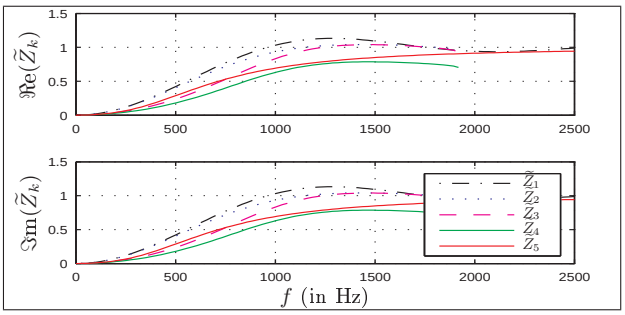

Figure 4. Impedance radiation comparisons for $R^\dagger$ at $z^\star$.

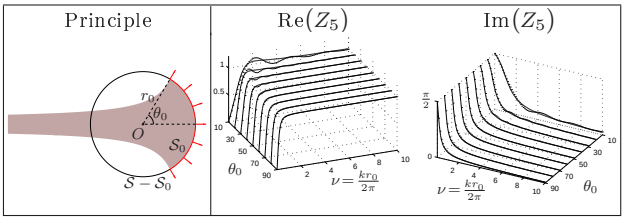

Figure 5. Flared horn radiation approximation, impedance averaged on $\mathcal{S}_0$ (...) and second order model Z_5 (-).

pipes (with radius a), have been established and compared (see e.g. [21]). They are usually described by

$$\frac{P_L}{V_L} = Z_{rad} = \rho c_0\,\widetilde{Z} \tag{9}$$

where $\widetilde{Z}$ is dimensionless and given as a function of $ka = (2\pi f/c_0)a$ (the wave number k maps to the imaginary Laplace variable $s = 2i\pi f = ikc_0/a$). Typical choices for $\widetilde{Z}$ are (see Figure 4): a caricatural real constant impedance $Z_0 \geq 0$, a flanged piston $Z_1 = 1 - \frac{2J_1(2ka)}{2ka} - i\frac{2H_1(2ka)}{2ka}$ (J_1 and H_1 are the Bessel and Struve function of first order), a flanged pipe Z_2 [21, (9)], an unflanged pipe Z_3 [22, (V.16)].

Nevertheless, radiation impedances of straight pipes are not well-adapted to flared horns. To take account of spherical wavefronts, a correction factor deduced from the energy and the mass conservation been proposed in [23] so that it recovers an exact result on $\Re\mathrm{e}(Z_4)$ when $f \to 0$ It yields yields $Z_4 = \frac{sin^2\theta_0}{2(1-\cos\theta_0)}Z_3$ where $\theta_0 \approx 59.2$ is the slope angle of $R^\dagger$ at $z = z^\star$.

To enhance the latter result, a model based on a portion $\mathcal{S}_0$ of a sphere $\mathcal{S}$ with radius r_0, pulsating with a uniform velocity V_0, has been proposed in [24] (see Figure 5). To be compatible with the curvilinear horn model, the pressure is averaged on $\mathcal{S}_0$, which yields a closed-form formula [24, (23)] of the load impedance. In this model, it is observed that:

(P4) *The ripples in straight pipe radiation impedances disappear for flared horns, if θ_0 is larger than about 55°. Radiation impedances are lower for spherical cases than for planar ones.*

In this configuration typical of many brass instruments, the impedance is accurately approximated by the second order model (the error is negligible w.r.t. to that due to the average) [24, (31)],

Table I. Regularity of the reflection functions involved in Kelly-Lochbaum structures w.r.t. the geometry regularity.

Approximation of $\mathcal{R}^\dagger$	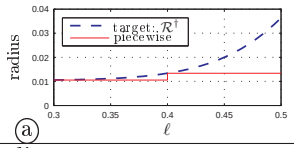 ⓐ	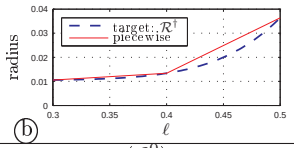 ⓑ	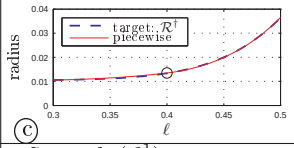 ⓒ
Profile regularity	discontinuous (straight pipes)	continuous ($\mathcal{C}^0$) (conical pipes)	Smooth ($\mathcal{C}^1$) (Υ-constant)
$R_{1,2}(s)$	$k_{1,2}=\frac{A_1-A_2}{A_1+A_2}$	$\frac{\alpha_{1,2}}{s-\alpha_{1,2}}$	$\frac{\Gamma_1(s)-\Gamma_2(s)}{\Gamma_1(s)+\Gamma_2(s)}$
$r_{1,2}(t)=$	$k_{1,2}\,\delta(t)$	$\alpha_{1,2}\,\exp(\alpha_{1,2}t)\,1_{t\geq 0}$	no closed-form solution
Jump at $t=0$	infinite ($k_{1,2}\delta'$)	$\alpha_{1,2}$	0
IR regularity	Dirac type	discontinuous	continuous ($\mathcal{C}^0$)

$$Z_5:\nu=\frac{kr_0}{2\pi}\longmapsto\frac{i\alpha\frac{\nu}{\nu_c}-\left(\frac{\nu}{\nu_c}\right)^2}{1+2i\xi\frac{\nu}{\nu_c}-\left(\frac{\nu}{\nu_c}\right)^2},\qquad(10)$$

with $\xi(\theta_0)=0.0207\theta_0^4-0.144\theta_0^3+0.221\theta_0^2+0.0799\theta_0+0.72$, $\alpha(\theta_0)=\left[0.1113\theta_0^5-0.6360\theta_0^4+1.162\theta_0^3-1.242\theta_0^2+1.083\theta_0+0.8788\right]^{-1}$ and $\nu_c(\theta_0)=\left[-0.198\theta_0^5+0.2607\theta_0^4-0.424\theta_0^3-0.07946\theta_0^2+4.704\theta_0+0.022\right]^{-1}$ (θ_0 is in radians).

5. Visco-thermal losses

Kirchhoff, first, has introduced thermal conduction effects, extended the Stoke's theory and derived some basic solutions in the free space and in a pipe. He gave the exact general dispersion relation for a cylinder for axisymmetric problems [25] (a generalized formula for non symmetric versions is given in [26, eq. (56)]).

Simplified models have also been proposed: separated viscous and thermal boundary layers (by Zwikker and Kosten [27, p.210], see [28, 29] for validity conditions), and the Cremer's equivalent wall admittance for plane waves [30] (which coincides with the Kirchhoff's result for rectangular waveguides such that the boundary layer thickness is much lower than the rectangle lengths).

Plane wave equations including these models have been derived, which include a damping term involving a fractional time derivative (see the Lokshin equation [31] and [32]). Exact solutions of the Lokshin equation have been derived in [33].

Adapting hypothesis (H1) in § 2 to the case of walls with a Cremer's wall admittance, a perturbed curvilinear version of (3) is obtained [12]. It is given by

$$\left(\partial_\ell^2+2\frac{\mathcal{R}'(\ell)}{\mathcal{R}(\ell)}\partial_\ell-\frac{1}{c^2}\partial_t^2-\frac{2\varepsilon(\ell)}{c^{\frac{3}{2}}}\partial_t^{\frac{3}{2}}\right)p(\ell,t)=0,\qquad(11)$$

where $\partial_t^{\frac{3}{2}}$ is a fractional time derivative [33] and $\varepsilon(\ell)=\kappa_0\frac{\sqrt{1-\mathcal{R}'(\ell)^2}}{R(\ell)}$ quantifies the visco-thermal effects ($\kappa_0=\sqrt{l'_v}+(\gamma-1)\sqrt{l_h}\approx 3\times10^{-4}\,\mathrm{m}^{1/2}$ in the air). This equation is sometimes called the "Webster (case $\varepsilon=0$)-Lokshin (case $R'=0$)" equation.

Considering Υ-constant segments on which $\ell\mapsto\varepsilon(\ell)$ is approximated by its mean value, results obtained in § 3 are generalized by replacing equation 7 by (for segment number n)

$$\Gamma(s)^2=\left(\frac{s}{c}\right)^2+2\varepsilon_n\left(\frac{s}{c}\right)^{\frac{3}{2}}+\Upsilon_n.\qquad(12)$$

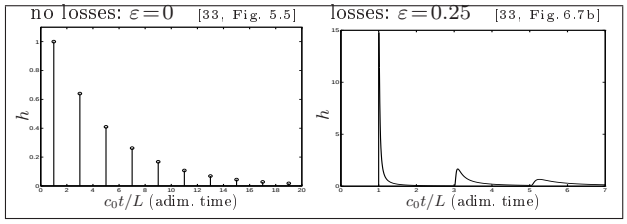

Figure 6. Pressure transmission IR ($p(L,t)=h*_t p(0,t)$) for a straight pipe loaded with a positive impedance at $z=L$.

Moreover, it has been proved that, even for constant piecewise profiles [33] (case ⓐ in Table I):

(**P4**) *The fractional derivative in equation 11 regularizes the impulse response of the input impedance, global reflection and transmission. It also makes long memory responses appear (decays slower than any decreasing exponential): Dirac pulses are transfromed in $\mathcal{C}^\infty$-pulses which increase fastly first and decay with long memory response (see Figure 6).*

6. Application and results

In this section, results due to §2-5 are compared to a reference, that is, a measured trombone bell. In Figure 7ⓐ, $\mathcal{C}^1$-regular Υ-constant decompositions of the measured profile are accurately optimized [20] with 5 segments for z- and ℓ- models (junction localizations $\circ$ correspond to $\ell\in\{0.2;0.4;0.48;0.55\}$ in m).

In Figure 7ⓑ, the input impedance (Mref) measured by the set up detailed in [1] is compared to the refined model (RM) based on the curvilinear $\mathcal{C}^1$-regular, piecewise Υ-constant, lossy propagation model connected to the radiation impedance Z_5. To exhibit the contribution of each refinement, modifications are introduced separately on (RM): (ZM) use of (z,R) rather than $(\ell,\mathcal{R})$; (FP) use of Z_1 (flanged piston) rather than Z_5; (NL) no losses ($\kappa_0=0$). Models (ZM) and (FP) yield significant peak deviations on amplitudes and frequencies for $f>600\,\mathrm{Hz}$, and (NL) emphasizes the peak amplitudes as expected.

Finally, Figure 7ⓒ corroborates results (R1) and (R2): : the piecewise conical approximations eventually recover the accuracy of (RM) when refining the mesh (here, for 40 cones).

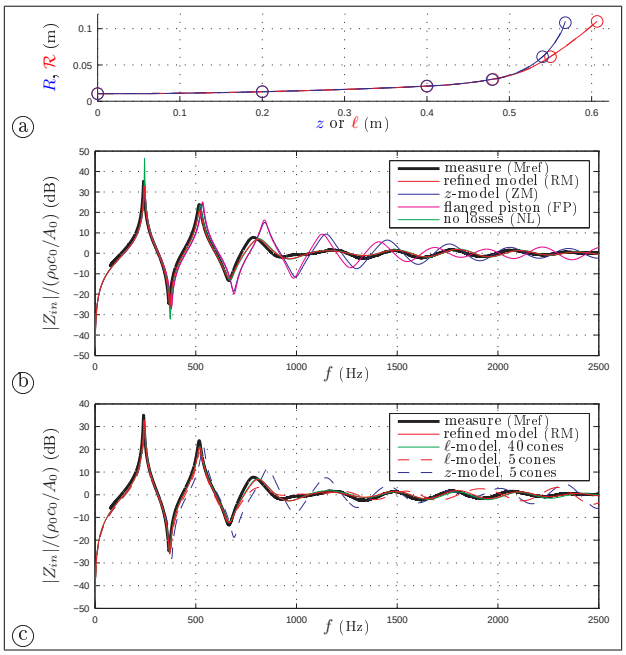

Figure 7. Results on a measured trombone bell.

7. CONCLUSIONS

The use of $\mathcal{C}^1$-*regular junctions of* Υ-*constant segments governed by the curvilinear Webster-Lokshin model* connected to the radiation impedance of a *pulsating portion of a sphere* proves to be relevant for the computation of the input impedance of smooth bores. This is the result of the 4 refinements proposed in sections 2 to 5 (in the sense that removing one of them yields worse results). Compared to the continuous piecewise conical segments, the $\mathcal{C}^1$-regular junctions of Υ-constant segments allow to significantly reduce the number of segments (other techniques can be found in [34]). This is not a critical point for the input impedance prediction from a profile, but it becomes the case for e.g. impedance optimization tools or sound synthesis purposes.

Acknowledgement

The authors thank P. Eveno and R. Caussé who have furnished the measures, as well as J. Kergomard and J.-P. Dalmont for bibliographic information.

References

[1] C.-A.Macaluso and J.-P. Dalmont. Trumpet with near-perfect harmonicity: Design and acoustic results. *JASA*, 129(1):404–414, 2011.

[2] J. L. Lagrange. Nouvelles recherches sur la nature et la propagation du son. Misc. Taurinensia (Mélanges Phil. Math., Soc. Roy. Turin), 1760-1761.

[3] D. Bernoulli. Sur le son et sur les tons des tuyaux d'orgues différemment construits. Mém. Acad. Sci. (Paris), 1764.

[4] A. G. Webster. Acoustical impedance, and the theory of horns and of the phonograph. *Proc. Nat. Acad. Sci. U.S.*, 5:275–282, 1919. Errata, ibid. **6**, p.320 (1920).

[5] E. Eisner. Complete solutions of the Webster horn equation. *JASA*, 41(4):1126–1146, 1967.

[6] R. F. Lambert. Acoustical studies of the tractrix horn. I. *JASA*, 26(6):1024–1028, 1954.

[7] E. S. Weibel. On Webster's horn equation. *JASA*, 27(4):726–727, 1955.

[8] A. H. Benade and E. V. Jansson. On plane and spherical waves in horns with nonuniform flare. I. Theory of radiation, resonance frequencies, and mode conversion. *Acustica*, 31:79–98, 1974.

[9] J. Agulló, A. Barjau, and D. H. Keefe. Acoustic propagation in flaring, axisymmetric horns: I. A new family of unidimensional solutions. *Acustica*, 85:278–284, 1999.

[10] G. R. Putland. Every one-parameter acoustic field obeys Webster's horn equation. *J. Audio Eng. Soc.*, 6:435–451, 1993.

[11] P. A. Martin. On webster's horn equation and some generalizations. *JASA*, 116(3):1381–1388, 2004.

[12] T. Hélie. Mono-dimensional models of the acoustic propagation in axisymmetric waveguides. *JASA*, 114:2633–2647, 2003.

[13] J. O. Smith. Physical modeling using digital waveguides. *Computer Music Journal*, 16:74–91, 1992.

[14] R. Mignot, T. Hélie, and D. Matignon. Digital waveguide modeling for wind instruments: building a state-space representation based on the webster-lokshin model. *IEEE TASLP*, 2010.

[15] T. Hélie, R. Mignot, and D. Matignon. Waveguide modeling of lossy flared acoustic pipes: Derivation of a kelly-lochbaum structure for real-time simulations. In *IEEE WASPAA*, pages 267–270, Mohonk, USA, 2007.

[16] T. Hélie and D. Matignon. Diffusive representations for analyzing and simulating flared acoustic pipes with visco-thermal losses. *M3AS*, 16-4:503–536, 2006.

[17] K.L. Kelly and C.C. Lochbaum. Speech synthesis. In *ICA*, pages 1–4, Copenhagen, Denmark, 1962. ICA.

[18] V. Välimäki. *Discrete-Time Modeling of Acoustic Tubes Using Fractional Delay Filters*. PhD thesis, Helsinki University of Technology, Faculty of Electrical Engineering, 1995.

[19] J.-D. Markel and A. H. Gray. *Linear prediction of speech*. Springer-Verlag, Berlin ; New York, 1976.

[20] T. Hélie, T. Hézard, and R. Mignot. Input impedance computation for wind instruments based upon the webster-lokshin model with curvilinear abscissa. In *ISMA*, Sydney, Australia, 2010.

[21] F. Silva, P. Guillemain, J. Kergomard, B. Mallaroni, and A.-N. Norris. Approximation of the acoustic radiation impedance of a cylindrical pipe. *Journal of Sound and Vibration*, 322:255–263, 2009.

[22] H. Levine and J. Schwinger. On the radiation of sound from an unflanged circular pipe. *Physical Review*, 73:383–406, 1948.

[23] R. Caussé, J. Kergomard, and X. Lurton. Input impedance of brass musical instruments - comparison between experiment and numerical models. *JASA*, 75:241–254, 1984.

[24] T. Hélie and X. Rodet. Radiation of a pulsating portion of a sphere: application to horn radiation. *Acta Acustica*, 89:565–577, 2003.

[25] G. Kirchhoff. Ueber die Einfluss der Wärmeleitung in einem Gase auf die Schallbewegung. *Annalen der Physik Leipzig*, 134, 1868. (English version: R. B. Lindsay, ed., Physical-Acoustics, Dowden, Hutchinson and Ross, Stroudsburg, 1974).

[26] M. Bruneau, P. Herzog, J. Kergomard, and J.-D. Polack. General formulation of the dispersion equation bounded visco-thermal fluid, and application to some simple geometries. *Wave motion*, 11:441–451, 1989.

[27] A. Chaigne and J. Kergomard. *Acoustique des instruments de musique*. Belin, 2008.

[28] J. Kergomard. *Champ interne et champ externe des instruments à vent*. Université Pierre et Marie Curie. Thèse d'Etat, 1981.

[29] J. Kergomard. Comments on wall effects on sound propagation in tubes. *J. Sound Vibr.*, 98(1):149–153, 1985.

[30] L. Cremer. On the acoustic boundary layer outside a rigid wall. *Arch. Elektr. Uebertr. 2*, 235, 1948.

[31] A. A. Lokshin and V. E. Rok. Fundamental solutions of the wave equation with retarded time. *Dokl. Akad. Nauk SSSR*, 239:1305–1308, 1978. (in Russian).

[32] J.-D. Polack. Time domain solution of Kirchhoff's equation for sound propagation in viscothermal gases: a diffusion process. *J. Acoustique*, 4:47–67, 1991.

[33] D. Matignon. *Représentations en variables d'état de modèles de guides d'ondes avec dérivation fractionnaire*. PhD thesis, Université de Paris XI Orsay, 1994.

[34] P. Eveno, J.-P. Dalmont, R. Caussé, and J. Gilbert. Comparisons between models and measurements of the input impedance of brass instruments bells. In *Forum Acusticum*, 2011.